Journal of Sound and Vibration 326 (2009) 161–176

Contents lists available at ScienceDirect

Journal of Sound and Vibration

journal homepage: www.elsevier.com/locate/jsvi

Attenuation of low frequency duct noise by a flute-like silencer ☆

Lixi Huang

Department of Mechanical Engineering, The University of Hong Kong, Pokfulam Road, Hong Kong

ARTICLE INFO

Article history:
Received 27 May 2008
Received in revised form
1 May 2009
Accepted 3 May 2009
Handling Editor: K. Shin
Available online 31 May 2009

ABSTRACT

A broadband, duct noise reflection mechanism is introduced in this theoretical study. It consists of side-branch cavities filled with a light gas, e.g. helium, and covered by impervious, tensioned membranes as two apertures, one at the inlet and another at the exit. Incident waves are scattered by the membranes into two passages, one through the central duct and another through the cavity bypass. Due to the faster speed of sound in the bypass, a Herschel–Quincke tube resonance appears and gives a peak in the transmission loss spectrum. Another resonance occurs when the frequency of the incident sound coincides with the vibroacoustic frequency determined by the membrane tension and inertia contributions from the membrane and the fluid media. With appropriate tensile stress, the trough between the two spectral peaks can be elevated to a desirable high level, e.g. 10 dB, and the crucial factor is identified as the low density of the cavity gas filling. The broadband sound reflection performance is comparable with and even exceeds that of the drum-like silencer [L. Huang, Parametric study of a drum-like silencer, *Journal of Sound and Vibration* 269 (2004) 467–488] with the same cavity geometry, but the current mechanism requires a low tensile stress which is much easier to implement in practice.

1. Introduction

Low frequency noise is often dominant in the environmental noise spectrum. In the well established noise criterion (NC) curve [1], the sound pressure level increases by about 6 dB when the frequency is halved in the region below about 500 Hz. Fortunately, the human hearing sensitivity also drops when frequency reduces. If one takes the A-weighting curve as a rough guide for such hearing sensitivity variation, the slope of 6 dB/octave is roughly matched by that of the A-weighting curve from 250 to 500 Hz. The main motivation for developing the technique of low frequency noise control is the current lack of effective passive control method. Using the traditional duct lining along a typical ventilation duct of 30 cm in dimension as an example, the typical attenuation rate for a noise of 100 Hz is about 5 dB/m of lining (cf. Fig. 9.22 of [2]). This rate drops rapidly as frequency further decreases. In fact, untreated low frequency noise, such as that in the octave bands of 63 and 31 Hz, could cause uncomfortable vibration of light-weight structures, which is the familiar rumbling near many air handling facilities. This problem is highlighted by the recently developed RC curves mark II [3], and is also elucidated very well in a recent review on room noise control [4].

Traditionally, passive control of low frequency noise relies heavily on the structural resonance; membrane and plate have been used in many cases and their main effect has been the mass required to achieve such low frequency resonance,

☆ Part of this work, mainly the result of Section 2, was presented at the 16th International Congress on Sound and Vibration, 5–9 July 2009, at Kraków, Poland.

E-mail address: lixi@hku.hk

0022-460X/$ - see front matter © 2009 Elsevier Ltd. All rights reserved.
doi:10.1016/j.jsv.2009.05.004

e.g. [5–7]. Recently, however, a different approach has been proposed by our group [8–14], which utilizes the full sound-structure coupling to achieve a broadband control in the low frequency region. As shown in Fig. 1(a), the basic prototype tested [10] resembles an expansion chamber with two side-branch cavities, each covered by a tensioned membrane. Incident sound wave induces the membrane to vibrate, and the vibration radiates secondary sound waves into both upstream and downstream. The upstream radiation represents sound reflection, while the downstream radiation interferes destructively with the incident wave, leading to noise attenuation in the downstream region. The acoustics of this interference is similar to that of a working rig of active duct noise control. The difference, which is an important one, is that the drum-like silencer is purely reactive and the destructive interference is guaranteed since the incident wave is the sole source of sound power. In order to achieve a broad stop-band, the tension required is typically on the same order of magnitude of the tensile strength of metallic alloys, hence the name 'drum-like'. This is explained as follows. The sound induced membrane vibration may be expanded into *in vacuo* modes described by displacement $\eta_j \propto \sin(j\pi x/L)$, where L is the membrane length and j is the mode number. The first *in vacuo* mode, $j = 1$, is effective in generating reflecting sound, but is difficult to excite due to the air stiffness in a compact cavity, the compactness being a desirable design attribute. In other words, the cavity volume controls the first mode. The second *in vacuo* mode, $j = 2$, is easier to excite but is less effective in reflecting sound as it is a dipole-like radiator. The effectiveness of the second mode depends on the ratio of the membrane length to the wavelength. In other words, it requires long membranes to reflect low frequency waves. For long membranes to respond in low order modes, high tension is required to keep the membrane to vibrate together. It is clear that the required tension would exceed the tensile strength of the material if the reflection of very low frequency is desired. It is also discovered later that, when the membrane is replaced by a light and stiff plate [13], equivalent or even better broadband performance is possible, but the requirement of high stiffness together with low mass again stretches to the limit of existing bulk materials [14]. The current study is motivated by the search for an alternative device for very low frequency noise control without using materials to their limit. The search has revealed that the acoustic mechanism of the traditional Herschel–Quincke (HQ) tube, shown in Fig. 1(b), would help relieve such limitation. The resulting device has a mechanism which is quite different from that of the drum-like silencer, and its appearance resembles the musical instrument of flute.

The device of Herschel–Quincke tube was introduced in the 19th century and its theory [15] has recently been re-examined [16]. When the length of the bypass, L_b in Fig. 1(b), is exactly half of a wavelength longer than the main passage (L_d), $L_b - L_d = \lambda/2$, where λ is the wavelength, the bypass plus this segment of the main duct becomes an acoustic branch with zero impedance seen by the incident wave. All sound waves are reflected. When $L_d \to 0$, the HQ tube is reduced to the standard quarter-wavelength resonator, shown in Fig. 1(c), the physics of which is somewhat easier to comprehend. For the HQ tube with the bypass having the same cross section as the main duct, the following physical explanation may be offered without involving the complex details of a full analysis presented in Section 2. Sound waves transmitted through the upstream junction propagate through the main duct and the bypass, and reach the downstream junction for further transmission to the exit duct. The transmitted waves from the two routes differ by a phase angle of π and cancel each other.

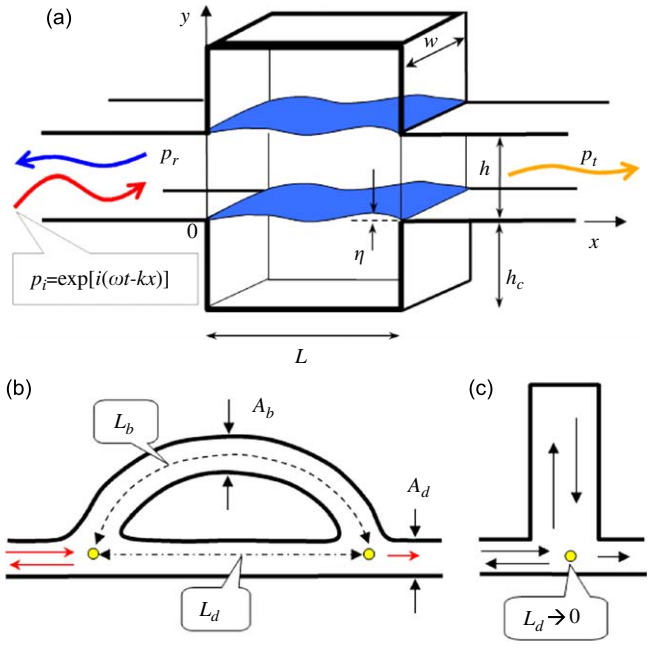

Fig. 1. Reactive silencers: (a) drum-like silencer [13], (b) Herschel–Quincke tube, which is equivalent to (c) a quarter-wavelength resonator when the duct passage length L_d vanishes.

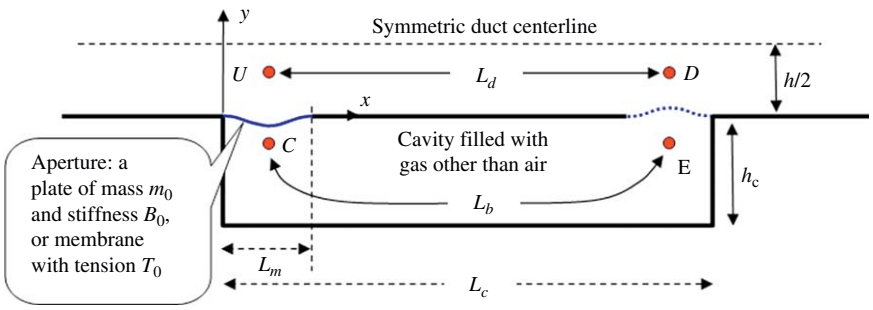

Fig. 2. Illustration of a symmetric half of a flute-like silencer.

The downstream junction is a pressure nodal point in a standing wave, and no transmitted wave is actually found in the exit duct. The two waves approaching the downstream junction simply proceed to the opposite passage and eventually return to the upstream junction, having gone through exactly the same total length of L_d+L_b. Further reflections by the upstream junction repeat what is described above. A second type of resonance occurs when the two routes combine to form an exact number of wavelength, e.g. $L_b + L_d = \lambda$. Similarly, zero transmitted wave is found in the exit duct, which is in effect also ignored by the waves passing through the downstream junction. Details of what happens in this resonance differ from that of type-1, and its physics will be explained in Section 2 after the basic equations needed, Eq. (1), are established and interpreted.

In an effort to reduce the membrane tension required by the drum-like silencer shown in Fig. 1(a), the long membrane is now broken into two short pieces and set apart by a segment of solid wall. The new configuration is shown in Fig. 2 for the lower symmetric half. Without the membranes, the device resembles an HQ tube in which the bypass is completely aligned with the duct segment. The use of the membranes also provides a possibility that the bypass can be filled with a gas other than the ambient fluid in the main duct, namely air. When a light gas, such as helium, is used, the wave propagation through the bypass is faster than that in the main duct since the bypass has essentially the same length as the main duct. When the time difference between the two acoustic routes becomes half of a period, a resonance peak is expected to occur in a way similar to that of the first type HQ resonance. It is shown in this study that another spectral peak appears when the membrane resonates with the fluids in the bypass and in the main duct, or when the inertance of the membrane and fluids is balanced by the effect of membrane tension. The trough between the two spectral peaks can be made much higher than that between two neighbouring HQ resonance peaks. The new device resembles the musical instrument of flute and the membranes will be called apertures. Similar to the drum-like silencer, the membrane aperture can also be replaced by a plate, but, unlike drum-like silencer, it is found that there is no difference in performance between the two types of apertures, and the choice can be made by implementation convenience.

In what follows, Section 2 analyses the problem shown in Fig. 2 based on the plane-wave assumption suitable for the low frequency regime. The results are then validated and improved in Section 3 by a full numerical solution. The effects of various aperture design, and the deviation between the plane-wave solution and the full numerical solution, are examined before conclusions are drawn in Section 4.

2. Plane-wave analysis

As shown in Fig. 2, the duct has a height of h and only the lower symmetric half of height $h/2$ is analysed in this problem. The cavity has a length of L_c and a depth of h_c. Most of the cavity length is separated from the duct by a solid wall except two apertures, each with length L_m, one at the upstream and another at the downstream ends of the cavity. The apertures are covered by impervious membranes so that a gas medium different from air can be filled in the cavity. It is shown later that the effects of mass and stiffness from the two membranes are essentially additive; simplified analysis may also be performed by assuming one of the two membranes to be massless and without tension. For the purpose of the plane-wave analysis for low frequencies, the pressure at the upstream region is represented by that at a point 'U' and the downstream region 'D'. The distance between the two is L_d through the duct and L_b through the bypass. If the points of 'U' and 'D' are assumed to be at the centres of the two membranes, the bypass length may be approximated by $L_b \approx L_c - L_m$. However, this approximation can only be tested by the full numerical solution in the next section. Length L_b is treated as a parameter in this section, while L_c is considered in the next section.

Consider the wave propagation for a general 1D passage with uniform cross section, fluid density ρ and speed of sound c. Between any two points at $x = x_1$ and x_2, a standing wave is formed by a right-travelling wave of linear pressure amplitude I and a left-travelling wave of amplitude R. The amplitudes I and R can be found by the pressures measured at the two points, p_1 and p_2,

$$p_1 = I\mathrm{e}^{-\mathrm{i}kx_1} + R\mathrm{e}^{+\mathrm{i}kx_1}, \quad p_2 = I\mathrm{e}^{-\mathrm{i}kx_2} + R\mathrm{e}^{+\mathrm{i}kx_2}.$$

Therefore,

$$I=\frac{p_1 e^{ikx_2}-p_2 e^{ikx_1}}{e^{ik(x_2-x_1)}-e^{-ik(x_2-x_1)}},\quad R=\frac{p_2 e^{-ikx_1}-p_1 e^{-ikx_2}}{e^{ik(x_2-x_1)}-e^{-ik(x_2-x_1)}}.$$

Here, and in all subsequent formulations, the time dependence of $\exp(i\omega t)$ is assumed and $k=\omega/c$ is the wavenumber. The acoustic particle velocity at the two points, u_1 and u_2, are found in terms of p_1 and p_2,

$$u_1=\frac{Ie^{-ikx_1}-Re^{+ikx_1}}{\rho c},\quad u_2=\frac{Ie^{-ikx_2}-Re^{+ikx_2}}{\rho c}.$$

Substituting expressions for I and R, the following equations are obtained:

$$u_1=\frac{p_1\cos\theta-p_2}{i\rho c\sin\theta},\quad u_2=\frac{p_1-p_2\cos\theta}{i\rho c\sin\theta},\tag{1}$$

where $\theta=k(x_2-x_1)$ is the phase difference, or angular distance.

Eq. (1) shall be used below to explain the physics of HQ tube resonance. It is necessary to build the right physical intuition from a full interpretation of these results. First of all, the results are most conveniently seen as a direct application of Newton's second law of motion, in which the pressure difference at the two points, 1 and 2, gives the net force applied per unit duct cross section, and the product of velocity u_1, u_2 with the denominator, $i\rho c\sin\theta$, can be rewritten as follows:

$$u(i\rho c\sin\theta)=[\sin(\theta)/\theta][\rho(x_2-x_1)]\partial u/\partial t.$$

The right-hand side of the above expression represents the inertia for the whole chunk of air between the two points with effective mass modified by a factor of $\sin\theta/\theta$. This mass modification factor accounts for the fact that not all particles are moving in step and particles at nodal points do not move at all. For very short length, $x_2-x_1\to 0$, the chunk of air conducts rigid-body motion with the familiar momentum equation recovered, $\rho(x_2-x_1)\partial u_1/\partial t\approx(p_1-p_2)$. The mass modification factor $\sin\theta/\theta$ tends to unity for such short length, and this settles the question of why the factor should involve $\sin\theta$ instead of $\cos\theta$, and that the pressure modification factor in the numerator should be $\cos\theta$, instead of $\sin\theta$,. The last question to be settled is why the pressure modification factor $\cos\theta$ is applied on p_1 when u_1 is calculated, or on p_2 when u_2 is calculated, cf. Eq. (1). This is best appreciated by considering the special case of a quarter-wavelength $\theta=\pi/2$ when Eq. (1) predicts $u_1=-p_2/(i\rho c)$. If point 2 is a rigid wall where the amplitude of p_2 reaches its maximum, point 1 should be a velocity maximum while point 2 is a velocity nodal point. It is evident that the way the pressure modification factor is applied is consistent with the common observation that pressure and velocity peak at different points in a standing wave, whose behaviour differs from a chunk of rigid body.

As mentioned in Section 1, type-2 HQ tube resonance occurs when the combined length of the bypass and the main duct forms one complete wavelength, $L_b+L_d=\lambda$, where L_b and L_d are shown in Fig. 1(b), for the simple configuration in which the bypass has the same cross section as the main duct, $A_b=A_d$. Denote the angular distance for the two passages as $\theta_d=kL_d$ and $\theta_b=kL_b=2\pi-\theta_d$, the rate of total volume flow arriving at the downstream junction, denoted as point 2, from the two passages is

$$Q_2=A_d\frac{p_1-p_2\cos\theta_d}{i\rho c\sin\theta_d}+A_b\frac{p_1-p_2\cos\theta_b}{i\rho c\sin\theta_b},$$

where p_1 and p_2 are the pressures at the upstream and downstream junctions, respectively. The relationship $\theta_b=2\pi-\theta_d$ means that $\cos\theta_b=\cos\theta_d, \sin\theta_b=-\sin\theta_d$, and that the two components of the volume flow amount to a total of zero, $Q_2=0$, when $A_b=A_d$. The main reason for such outcome, $\sin\theta_b=-\sin\theta_d$, reflects the fact that the total effective mass for the two branches is zero as the motion of all air particles in one wave cycle balances themselves out. With no volume flow into the downstream junction, no outflow is found in the exit duct as the waves arriving from the bypass at the downstream junction go back to the upstream junction through the main duct passage, while those through the main duct proceed to the bypass. In other words, the waves travel in a loop formed by the two branches and the exit duct is effectively ignored. It can be shown by the full analysis below that the strength of the two waves travelling in this loop is determined by the requirement that the downstream junction is a pressure node, and the upstream an anti-node. It is easily shown that the total volume flow leaving the upstream junction is also zero,

$$Q_1=A_d\frac{p_1\cos\theta_d-p_2}{i\rho c\sin\theta_d}+A_b\frac{p_1\cos\theta_b-p_2}{i\rho c\sin\theta_b}=0.$$

The upstream junction is a velocity nodal point in type-2 resonance.

Similar analysis for type-1 HQ resonance for $L_b=L_d+\lambda/2$ is less straight-forward but is still feasible. The volume flow converging towards the downstream junction

$$Q_2=A_d\frac{p_1-p_2\cos\theta_d}{i\rho c\sin\theta_d}+A_b\frac{p_1-p_2\cos\theta_b}{i\rho c\sin\theta_b}$$

becomes $Q_2=-2A_d(p_2\cos\theta_d/i\rho c\sin\theta_d)$ when the relationships of $\cos\theta_b=-\cos\theta_d, \sin\theta_b=-\sin\theta_d$ are used. This total volume flow has to flow out through the exit duct in which only one single travelling wave is allowed, in which case

the volume flow must be in phase with the junction pressure due to $p=\rho cu$ in the exit duct. Since the arriving volume flow, Q_2, is out of phase with p_2, as indicated by 'i' in the denominator of the above expression. The only possible outcome is $Q_2=0, p_2=0$, which is the same as for the type-2 resonance but for different reasons. This time, the total volume flow leaving the upstream junction does not vanish, $Q_1=A_d(2p_1\cos\theta_d/\mathrm{i}\rho c\sin\theta_d)\neq 0$, contrasting with the type-2 resonance.

Having offered the physical explanation for the traditional HQ tube resonance, the attention is now turned to the flute-like silencer. As shown in Fig. 2, four pressure taps are placed and they are labelled as '*U*', '*D*', '*C*' and '*E*' for the upstream, downstream, cavity upstream and cavity downstream regions, respectively. The pressure difference between '*U*' and '*C*', denoted as $\Delta p_{CU}=p|_{y=0-}-p|_{y=0+}$, drives the upstream membrane vibration, and that between '*D*' and '*E*' drives the downstream membrane vibration. It is shown below that the membranes can be replaced by plates and they can have the same performance with suitable parametric relations. For the upstream membrane occupying $x\in[0,L_m]$, the dynamics of the membrane vibration is written as

$$m_0\frac{\partial^2\eta}{\partial t^2}=T_0\frac{\partial^2\eta}{\partial x^2}+\Delta p_{CU},$$

where m_0 is the mass per unit axial length, T_0 the membrane tension per unit width in the direction perpendicular to the 2D plane being studied here. This equation may be integrated over its length,

$$m_0\omega^2\int_0^{L_m}\eta\,\mathrm{d}x+T_0\left(\frac{\partial\eta}{\partial x}\right)_{x=0}^{x=L_m}+\int_0^{L_m}\Delta p_{CU}\,\mathrm{d}x=0$$

to give the relationship between the integrated pressure forces and the rate of volume displacement by the vibrating membrane. To do so, it is tactically assumed, and later verified by the full numerical solution, that the fundamental mode of vibration dominates when the excitation frequency is low and the tension is sufficiently high. The displacement is $\eta\approx\eta_1\sin(\pi x/L_m)\mathrm{e}^{\mathrm{i}\omega t}$, where η_1 is the modal amplitude. Substituting this displacement into the above dynamics equation and letting

$$\int_0^{L_m}\Delta p_{CU}\,\mathrm{d}x=L_m(p_C-p_U),$$

where p_C and p_U are the local average values of pressure around '*C*' and '*U*', respectively, one obtains the complex amplitude of the mean upward vibration velocity

$$v_m=\frac{p_C-p_U}{\mathrm{i}m_0(\omega-\omega_1^2\omega^{-1})},\tag{2a}$$

where v_m is defined below together with the first mode *in vacuo* resonance frequency ω_1,

$$v_m=\frac{1}{L_m}\int_0^{L_m}\frac{\partial\eta}{\partial t}\,\mathrm{d}x\approx\frac{2}{\pi}(\mathrm{i}\omega\eta_1),\quad \omega_1=\frac{\pi}{L_m}\sqrt{\frac{T_0}{m_0}}.\tag{2b}$$

When a clamped plate is used, the dynamics equation and the solution for the *in vacuo* modes are given below,

$$B_0\partial^4\eta/\partial x^4+m_0\partial^2\eta/\partial t^2=0,\quad \eta(0)=\eta_x(0)=\eta(L_m)=\eta_x(L_m)=0,$$

$$\eta=C_1[\sin(k_px/L_m)-\sinh(k_px/L_m)]+C_2[\cos(k_px/L_m)-\cosh(k_px/L_m)],$$

where B_0 and m_0 are the plate stiffness per unit width and mass per unit axial length, respectively, k_p and C_2/C_1 take the following characteristic values:

$$\frac{k_p}{\pi}=1.5056,2.4998,3.5000,\quad \frac{C_2}{C_1}=\frac{\cos k_p-\cosh k_p}{\sin k_p+\sinh k_p}=-1.0178,-0.9992,-1.000$$

for the first three modes, respectively.

For the plate vibration driven by the acoustic pressure difference, the dynamics equation

$$B_0\partial^4\eta/\partial x^4-m_0\omega^2\eta=\Delta p_{CU}$$

is integrated for the assumed first mode to give the following mean vibration velocity:

$$v_m=\frac{1}{L_m}\int_0^{L_m}\frac{\partial\eta}{\partial t}\,\mathrm{d}x=\frac{p_C-p_U}{\mathrm{i}m_0(\omega-\omega_1^2\omega^{-1})},\quad \omega_1=\left(\frac{1.5056\pi}{L_m}\right)^2\sqrt{\frac{B_0}{m_0}}\tag{3}$$

which has the same form of pressure–velocity relationship as Eq. (2a).

The pressure at junction '*U*' is a combination of incident (I_0) and reflection (R_0) waves; while that downstream of junction '*D*' consists purely of the transmitted wave whose complex amplitude is denoted as p_D,

$$p|_{x\leq x_U}=I_0\,\mathrm{e}^{-\mathrm{i}k_0(x-x_U)}+R_0\,\mathrm{e}^{+\mathrm{i}k_0(x-x_U)},\quad p_U=I_0+R_0;\quad p|_{x\geq x_D}=p_D\,\mathrm{e}^{-\mathrm{i}k_0(x-x_D)},\tag{4a}$$

where $k_0=\omega/c_0$ is the wavenumber in the main duct. The acoustic particle velocity at the left-hand side of point 'U', denoted by u_{UL}, is $u_{UL}=(I_0-R_0)/(\rho_0 c_0)$, in which R_0 can be substituted by Eq. (4a), $R_0=p_U-I_0$, hence

$$\rho_0 c_0 u_{UL}=2I_0-p_U. \tag{4b}$$

The volume flow rate into point 'U' from upstream, $A_d u_{UL}$, where A_d is the duct cross section, or $h/2$ for the lower half of the 2D channel considered here, is divided into two streams: one flowing from 'U' to 'D', denoted as u_{UR}, which is derived from the general expression of Eq. (1), and another into the cavity at velocity $-v_m$, where v_m is given in Eq. (2a), or Eq. (3) for a plate. The volume flow conservation reads $\frac{1}{2}hu_{UL}=\frac{1}{2}hu_{UR}+L_m(-v_m)$, which becomes, after multiplying the specific impedance of the ambient fluid $\rho_0 c_0$, and utilizing Eqs. (1), (2a), and (4b),

$$\frac{h}{2}(2I_0-p_U)=\frac{h}{2}\times\frac{p_U\cos k_0L_d-p_D}{\mathrm{i}\sin k_0L_d}-L_m\rho_0c_0\frac{p_C-p_U}{\mathrm{i}m_0(\omega-\omega_1^2/\omega)}=0.$$

The above equation is rewritten as

$$2\mathrm{i}I_0=p_U(\mathrm{i}+\cot\theta_0+a_m)-p_D\csc\theta_0-p_Ca_m, \tag{5a}$$

where

$$a_m=\frac{2\rho_0c_0L_m/h}{m_0(\omega-\omega_1^2/\omega)}=\frac{2\rho_0L_m}{m_0}\left(\frac{\omega h}{c_0}-\frac{\omega_1^2h}{\omega c_0}\right)^{-1}\quad\text{and}\quad\theta_0=k_0L_d \tag{5b}$$

are the dimensionless membrane vibration admittance and the duct passage length in radian, respectively. The second volume flow continuity is the equality of the membrane velocity and the particle velocity in the cavity passage evaluated at the upstream end by substituting p_1 and p_2 in the u_1 expression of Eq. (1) by p_C and p_E:

$$-L_mv_m=h_c\frac{p_C\cos\theta_b-p_E}{\mathrm{i}\rho_cc_c\sin\theta_b},\quad\theta_b=k_cL_b,$$

where subscript 'c' signifies cavity in the above expression, $k_c=\omega/c_c$ is the wavenumber in the cavity, L_b the effective bypass length inside the cavity and θ_b the angular passage length in the bypass. Substituting v_m from Eq. (2a) into the above equation

$$a_mp_U-(a_m+a_c\cot\theta_b)p_C+(a_c\csc\theta_b)p_E=0, \tag{6a}$$

where

$$a_c=\frac{2\rho_0c_0h_c}{\rho_cc_ch} \tag{6b}$$

is a dimensionless acoustic admittance for the cavity passage. The third volume flow continuity is that the volume flow into the membrane at 'E' is the same as the volume displacement by the downstream membrane,

$$L_mv'_m=h_c\frac{p_C-p_E\cos\theta_b}{\mathrm{i}\rho_cc_c\sin\theta_b},\quad v'_m=\frac{p_E-p_D}{\mathrm{i}m'_0(\omega-\omega'^2_1/\omega)},$$

where primes distinguish the downstream membrane from the upstream one. Making use of the membrane admittance defined in Eq. (5b), one obtains

$$a'_mp_D-(a'_m+a_c\cot\theta_b)p_E+(a_c\csc\theta_b)p_C=0. \tag{7}$$

The last volume flow continuity at junction 'D' is similar to that at 'U': the cavity stream converges with the main duct stream at point 'D' and they form the transmitted wave downstream,

$$L_m\frac{p_E-p_D}{\mathrm{i}m'_0(\omega-\omega'^2_1/\omega)}+\frac{h}{2}\times\frac{p_U-p_D\cos\theta_0}{\mathrm{i}\rho_0c_0\sin\theta_0}=\frac{h}{2}\times\frac{p_D}{\rho_0c_0}.$$

The above equation is also rewritten as

$$a'_m(p_E-p_D)+p_U\csc\theta_0-p_D\cot\theta_0=\mathrm{i}p_D. \tag{8}$$

Eqs. (5a), (6a), (7) and (8) can be collected in a matrix form

$$\underbrace{\begin{bmatrix}\mathrm{i}+\cot\theta_0+a_m & -a_m & 0 & -\csc\theta_0\\ -a_m & a_m+a_c\cot\theta_b & -a_c\csc\theta_b & 0\\ 0 & -a_c\csc\theta_b & a'_m+a_c\cot\theta_b & -a'_m\\ -\csc\theta_0 & 0 & -a'_m & \mathrm{i}+\cot\theta_0+a'_m\end{bmatrix}}_{\mathscr{M}}\begin{bmatrix}p_U\\ p_C\\ p_E\\ p_D\end{bmatrix}=2\mathrm{i}I_0\begin{bmatrix}1\\0\\0\\0\end{bmatrix}, \tag{9}$$

where the coefficient matrix is denoted as $\mathscr{M}$. The set of equations can be solved for the pressure transmission ratio p_D/I_0,

$$\frac{p_D}{I_0}=\frac{2i\Delta_D}{\det(\mathscr{M})},\quad \Delta_D=\begin{vmatrix} -a_m & a_m+a_c\cot\theta_b & -a_c\csc\theta_b \\ 0 & -a_c\csc\theta_b & a'_m+a_c\cot\theta_b \\ \csc\theta_0 & 0 & a'_m \end{vmatrix}. \tag{10}$$

System resonance occurs when $p_D=0$, or $\Delta_D=0$, where Δ_D is expanded below,

$$\begin{aligned}\Delta_D &= a_m a'_m a_c\csc\theta_b+\csc\theta_0(a_m+a_c\cot\theta_b)(a'_m+a_c\cot\theta_b)-\csc\theta_0 a_c^2\csc^2\theta_b \\ &= a_m a'_m(a_c\csc\theta_b+\csc\theta_0)+\csc\theta_0 a_c\cot\theta_b(a_m+a'_m)-\csc\theta_0 a_c^2,\end{aligned}$$

and the resonance condition rewritten as

$$\frac{\Delta_D\sin\theta_0\sin\theta_b}{a_m a'_m}=(a_c\sin\theta_0+\sin\theta_b)+(z_m+z'_m)a_c\cos\theta_b-z_m z'_m a_c^2\sin\theta_b=0 \tag{11a}$$

with the introduction of the membrane impedance z_m defined below,

$$z_m=a_m^{-1}=\frac{m_0}{2\rho_0 L_m}\left(\frac{\omega h}{c_0}-\frac{\omega_1^2 h}{\omega c_0}\right),\quad z'_m=\frac{m'_0}{2\rho_0 L_m}\left(\frac{\omega h}{c_0}-\frac{\omega_1'^2 h}{\omega c_0}\right). \tag{11b}$$

These impedance terms vanish when a massless membrane without tension is assumed.

The resonance condition $\Delta_D=0$ is analysed below for two cases. First, when the two apertures are taken away, $z_m=z'_m=0$, and the device becomes a pure HQ tube, the first bracket term in the right-hand side of Eq. (11a) vanishes, which is listed below together with the definition of cavity admittance for easier analysis,

$$a_c\sin k_0 L_d+\sin k_c L_b=0,\quad a_c=(2\rho_0 c_0 h_c)/(\rho_c c_c h). \tag{12}$$

When the cavity is not filled with a different gas, $k_c=k_0$, and when the two bypass cross section combined is equal to the main duct height, $2h_c=h$, one has $a_c=1$ and Eq. (12) becomes $\sin k_0 L_d+\sin k_0 L_b=0$. As shown in [16] and mentioned also in Section 1, the first type of HQ tube resonance occurs when $k_0 L_d=k_0 L_b-(2n+1)\pi$, where n is an integer. In other words, when the differential path L_b-L_d is an odd multiple of $\lambda/2$. The second type of resonance occurs when $k_0 L_d=2n\pi-k_0 L_b$, or when the combined path L_b+L_d is an integer multiple of λ. If the cavity is filled with a light gas, and it is not much longer than the duct segment, $L_b\approx L_d$, the resonance condition requires $k_0 L_d$ to exceed π, or $L_d>\lambda/2$. Otherwise the bypass L_b must exceed half a wavelength. As shown below, this constraint is removed by the use of a membrane or plate aperture illustrated in Fig. 2.

Returning now to the resonance condition for the second case in which a membrane or plate aperture is employed. Not much further analysis can be made for Eq. (11a) to obtain a closed-form resonance frequency unless some knowledge is given for the aperture design. If a single aperture is used, $z'_m=0$, the condition of Eq. (11a) becomes

$$(z_m a_c)_{\text{single}}=-\frac{a_c\sin\theta_0+\sin\theta_b}{\cos\theta_b} \tag{13a}$$

which can be shown (see below) to give the single aperture resonance frequency ω_{single},

$$\omega^2_{\text{single}}\approx\frac{m_0\omega_1^2/L_m}{m_0/L_m+2\rho_0 L_d/h+\rho_c L_b/h_c}, \tag{13b}$$

provided that the resonance frequency is found in the low frequency region. If two identical apertures are used, $z_m=z'_m$, Eq. (11a) gives

$$(z_m a_c)_{\text{twin}}=\frac{\cos\theta_b}{\sin\theta_b}\left(1\pm\sqrt{1+\frac{\sin\theta_b(a_c\sin\theta_0+\sin\theta_b)}{\cos^2\theta_b}}\right). \tag{14}$$

Eqs. (14) and (13a) do not look similar in the first place, but can be shown to be similar when the resonance is again assumed to occur in the low frequency region. Using the approximation of $\sin x\approx x,\cos x\approx 1$ and expanding the square-root in Eq. (14),

$$(z_m a_c)_{\text{twin}}\approx\frac{2}{\theta_b},-\frac{a_c\theta_0+\theta_b}{2}.$$

The first of the two roots above is not a valid low frequency solution, but the second one is. Noting that z_m,θ_0,θ_b all contain ω, the second root can be rewritten for the low-frequency, twin-aperture solution,

$$\omega^2_{\text{twin}}\approx\frac{2m_0\omega_1^2/L_m}{2m_0/L_m+2\rho_0 L_d/h+\rho_c L_b/h_c} \tag{15}$$

which is similar to Eq. (13b) except that m_0 in the latter is replaced by $2m_0$ in Eq. (15). In both formulas, the product of $m_0\omega_1^2 = \pi^2 T_0/L_m^2$ is essentially the tensile force for the membrane, or $4.730^4 B_0/L_m^4$ for a plate. So, the numerator in Eq. (15) contains the combined structural restoring forces, and the denominator combines all terms of inertia. In other words, the effects of aperture masses and structural restoring forces are additive in the low frequency limit. The two fluid terms are proportional to the density and the length as the fluid in the whole length move in phase at low frequencies. They are inversely proportional to the channel width as wide channel means smaller velocity for a given volume flow rate. The same principle applies to the membrane term where denominator L_m represents a cross sectional width instead of passage length. The sum over the three inertia terms implies that the acoustic particle oscillation is circulating around the duct and through the cavity, very much like the second type of resonance in the HQ tube where the combined length $L_d + L_b$ is equal to the wavelength (when $A_d = A_b$). Note that such simplistic pattern of particle velocity is not found for any particular moment due to the presence of standing waves in both the duct segment and the bypass. Notice also that Eq. (15) is quantitatively valid only if the resonance frequency is very low.

The usual HQ tube resonance is expected to occur with modification by the aperture and cavity gas properties, but further simplified analysis is not as straight-forward. Solution for p_D in Eq. (10) can be computed without further approximation, and the results for the performance of pure HQ tube is given in Fig. 3 by setting $m_0 = m_0' = 0$ and tactically allowing different gas filling in the bypass. The downstream aperture shown in dashed line in Fig. 2 is intended to describe such hypothetic setting at an aperture. A bypass length of $L_b = 10h$ is assumed for all cases shown in Fig. 3, and the cavity filling is air for all but two curves in Fig. 3(c). Fig. 3(a) studies the effect of varying the ratio of the bypass cross section to the duct cross section, A_b/A_d. The thick dashed line is for $A_b/A_d = 1$, while the other two lines are for 0.75 and 1.25, respectively. The overall pattern repeats with a dimensionless frequency interval of $f = 0.2$, where f is defined below together with other dimensionless parameters,

$$f = \frac{\omega h}{2\pi c_0}, \quad m = \frac{m_0}{\rho_0 h}, \quad B = \frac{B_0}{\rho_0 c_0^2 h^3}, \quad T = \frac{T_0}{\rho_0 c_0^2 h}. \tag{16}$$

An example of dimensional size may be helpful here. For a duct of height $h = 0.3$ m, the dimensionless frequency of $f = 0.1$ means 113.3 Hz and a membrane mass ratio of $m = 0.25$ means a thickness of 0.034 mm for aluminium. As shown in Fig. 3(a), below $f = 0.2$, there are three peaks around $f = 0.2/3, 0.3/3, 0.4/3$ and they are the second, first and second types of HQ resonance, respectively. The middle peak is the first type resonance with the differential path of $L_b - L_d = \lambda/2$. When A_b increases, the trough between peaks is elevated as peaks move closer together, and the peaky spectrum becomes rather rounded, like that of an expansion chamber, when $A_b/A_d = 5$ (dash–dot line). In Fig. 3(b), a very short main duct length is set, $L_d = 0.5h$, while $L_b = 10h$ is kept unchanged. The spectrum is rather close to that of a standard quarter-wavelength resonator illustrated in Fig. 1(c). The first four peaks for the case of $A_b/A_d = 1$ are for the first type resonance ($L_b - L_b = \lambda/2$), second type resonance ($L_b + L_d = \lambda$), the higher-order first type resonance $L_b - L_b = 1.5\lambda$, and the higher-order second type resonance ($L_b + L_d = 2\lambda$), respectively. The spectral peak for the second type resonance is very narrow.

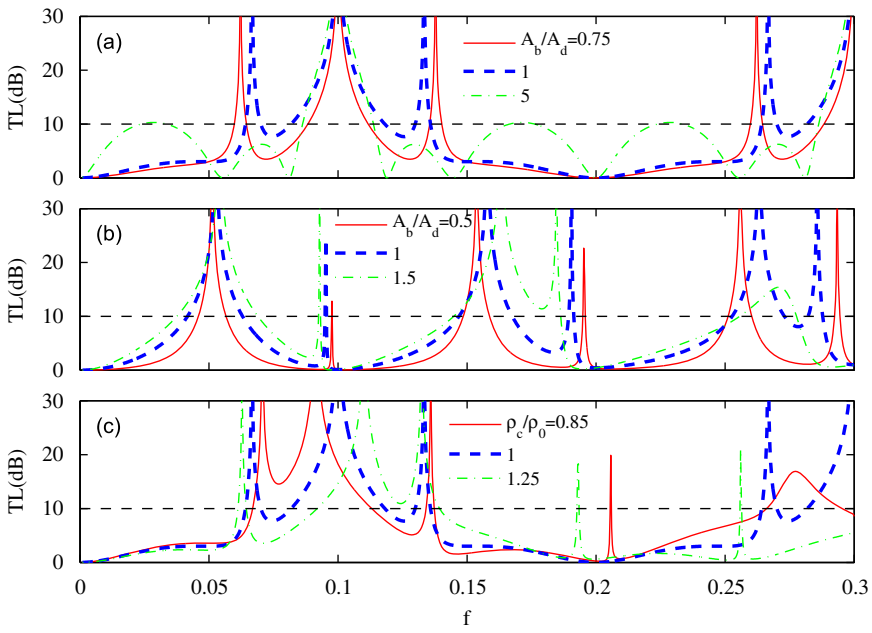

Fig. 3. The performance of the pure HQ tube: (a) effect of the bypass area, (b) reduction of HQ tube into a quarter-wavelength resonator, and (c) effect of bypass gas filling. The bypass length is $L_b = 10h$ for all cases.

Fig. 3(c) investigates the effect of cavity filling with different gases while the equilibrium or static pressure, P, is held the same as that in the main duct. Note that $P=\gamma\rho_c c_c^2$ and the ratio of specific heats, $\gamma=c_p/c_v$, can be different from that of air depending on the type of gas used. However, γ is chosen to be the same as air ($\gamma=7/5$) for this particular example since the gas is not actually specified, while that for helium follows its true value of $\gamma=5/3$ in later examples. It is clear from Eq. (12) that, when $\rho_c\downarrow, c_c\uparrow$, the effective bypass length is decreased due to the faster wave speed, as shown in $k_cL_b=\omega L_b/c_c$, while the effective bypass cross section is increased due to the decreased specific acoustic impedance $\rho_c c_c$, as shown by the parameter a_c which contains $h_c/(\rho_c c_c)$. In other words, in order to give exactly the same sound propagation time, the length of a helium bypass should be increased. It is possible to achieve exactly the same HQ tube performance with a longer but narrower bypass when a light gas is used, or a shorter and wider bypass when a heavy gas is used. When the effective length and cross section are not kept constant, resonance peaks shift, as shown in Fig. 3(c). It is shown below that, when an aperture is used, the effect of a different bypass gas can provide clear acoustic benefit instead of simple pattern shifts.

When at least one aperture made of a plate or a membrane is installed, the device becomes a flute-like silencer. A fluid-structure coupled resonance is expected to occur at a frequency approximated by Eq. (13b) for the single-aperture design, or Eq. (15) for the design of two identical apertures at the two ends of the bypass. The effect of the aperture can be investigated by comparing its spectrum of transmission loss (TL) with the same device without aperture ($z_m=z'_m=0$) but with the cavity filled with the same gas as described above. In Fig. 4, spectral comparison is made between such a single-aperture, flute-like silencer and the HQ tube of the same geometry and helium filling in the cavity. For the flute-like silencer, the following design parameters are adopted:

$$L_d=4h,\quad L_m=h,\quad A_b=2h_c,\quad h_c=h,$$

$$L_b=L_d-L_m+\pi h_c/2=4.057h,$$

$$\rho_c=0.13\rho_0,\quad c_c=3.0261c_0,\quad m=0.25, \tag{17}$$

where the bypass distance L_b is calculated heuristically by drawing a quarter of a circle of radius $h_c/2$ around points 'U' and 'D' in Fig. 2, respectively. Results for the two values of tension are shown in Fig. 4, $T=0.02$ and 0.042, the latter value being chosen to allow the trough between the first two peaks to exceed 10 dB. If such a 10 dB threshold is used, as was done for earlier studies on drum-like silencer of similar geometry [12], the stop-band is $f\in[0.031,\ 0.141]$ for $T=0.042$ (solid line in Fig. 4), with a bandwidth over two octaves, $0.141/0.031=4.6>4$. The first two peaks occur at $f=0.0343$ and 0.1352. The frequency of the first peak should be approximated by Eq. (13b), which gives $f=0.0345$. The approximation is very close to the actual resonance and is shown with a label '$f_{\rm res}$' in the figure. When the two-aperture design is used with the mass of $m=0.25$ divided into two halves, $m=0.125$ for each, a tensile stress level with $T=0.015$ is required to elevate the trough above 10 dB with almost identical overall TL pattern. However, the resonance frequency approximation of Eq. (15) under-predicts by about 15 percent, and the reason is that the location of the resonance peak does not really satisfy the 'low-frequency' assumption required to expand the square-root term in Eq. (14) by the simple Taylor series of $\sqrt{1+x}\approx 1+x/2$, which is valid only for $|x|<1$. That term involves the passage length which may not be very short compared with the

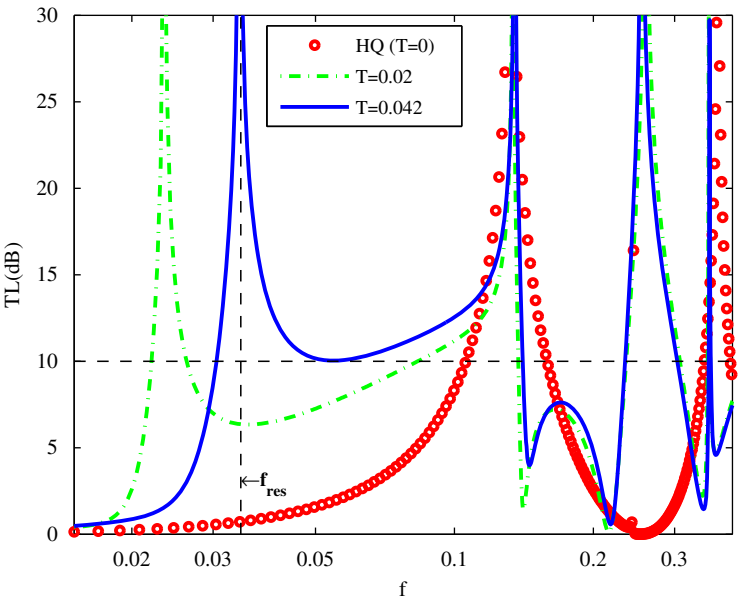

Fig. 4. Comparison between a twin-aperture, flute-like silencer with HQ tube, both with cavity filled by helium. Other design parameters are given in (17).

wavelength, but the failure of this particular expansion does not affect the overall validity of the low frequency approximation which only requires that the dimension of the cross section is much shorter than a wavelength.

The TL for the helium-filled HQ tube is found by setting $T = 0$, $m = 0$ in the code, and the result is shown in Fig. 4 as the line with open circles. It overlaps with the flute-like silencer for most of the frequencies around and higher than the second resonance peak of $f = 0.1325$. In other words, the aperture does not have much influence in this frequency regime, which can be explained as follows. The stiffness term is important only at very low frequencies, and the inertia term is important at higher frequencies but the dimensionless mass of $m = 0.25$ is low. When a much higher mass ratio is set, obvious deviation could appear. However, the TL performance would be rather poor and such design is of little practical interest and is thus excluded from further consideration. The effect of mass and issues of practical implementation are discussed in Section 4. The flute-like silencer with a lower level of tension $T = 0.02$ produces similar spectrum (dash–dot line) with a lower first resonance frequency. The second peak also overlaps with the HQ resonance and is almost unchanged.

The nature of the HQ tube resonance shown by the dash–dot line of Fig. 4 is further analysed as follows. The two resonance peaks shown in Fig. 4 are at $f = 0.1352$ and 0.2547, respectively. For the flute-like silencer shown in Fig. 2 with the bypass filled with helium, which has lower density and higher speed of sound, the effective acoustic path is shorter in the bypass as the wave speed is faster than that in the main duct. The HQ tube resonance condition, Eq. (11), is detailed as follows for the above two resonance frequencies:

$$a_c = 2h_c/(\rho_c c_c/\rho_0 c_0) = 2 \times 1/0.3934 = 5.0839,$$
$$k_0 L_d = 1.08\pi,\ 2.04\pi, \quad k_c L_b = 0.41\pi,\ 0.77\pi,$$
$$\sin(k_0 L_d) + a_c^{-1}\ \sin(k_c L_b) = 0.$$

The first resonance at $f = 0.1352$ corresponds to the type-1 HQ tube resonance when the differential path is $\lambda/2$ with $a_c = 1$. The second resonance at $f = 0.2547$ corresponds to the type-2 HQ tube resonance when the combined path is one wavelength and $a_c = 1$.

3. Numerical simulation of the 2D model

In this section, full numerical simulation is employed to confirm the qualitative conclusions reached by the 1D theory based on the plane-wave assumption suitable for low frequencies and the fundamental mode vibration for the aperture. The method of Chebyshev collocation with domain decomposition is employed. The 2D model is shown in Fig. 5 which also illustrates all the domain interfaces. The central symmetric line is treated as a hard wall. The half duct channel is divided into five rectangular domains while the cavity is divided into three. The aperture dynamics is enforced by the interface matching condition. The exit boundary satisfies the plane out-going wave condition appropriate for the low frequency application here, and the same is true for the reflected wave through the inlet. The two sides of an interface are assigned separate letters for easy identification of the boundary and the associated domain in computation, e.g. '*a*' and '*b*' are for $x = 0-$ and $x = 0+$, respectively, and they appear in the computation of two adjacent domains. The cavity side of the interface uses the upper case of the same alphabet used for the duct. The basic methodology of Chebyshev collocation and domain decomposition can be found in [17], and its implementation for a related but simpler geometry at high frequencies is described in [18]. The particular scheme used in this study is outlined below, followed by mesh convergence tests.

The Chebyshev collocation method is a spectral method and is implemented very much like a finite difference method on the special Gauss–Lobatto mesh of

$$\tilde{x}_n = -\cos(nx\pi/N), \quad n = 0, 1, 2, \ldots, N$$

when an interval is normalized to lie within $\tilde{x} \in [-1, +1]$. All variables are expanded in terms of the truncated Chebyshev series, and the derivatives can be expressed by products of derivative matrices with the column vectors for the entire line of mesh given above. By having more clustered grids near the domain boundaries, the Chebyshev expansion suppresses the large error oscillation at the end points which occurs in other high-order, global interpolation schemes [17]. The high accuracy is obtained at the expense of having to use fully populated matrices in the discretized system. The burden of

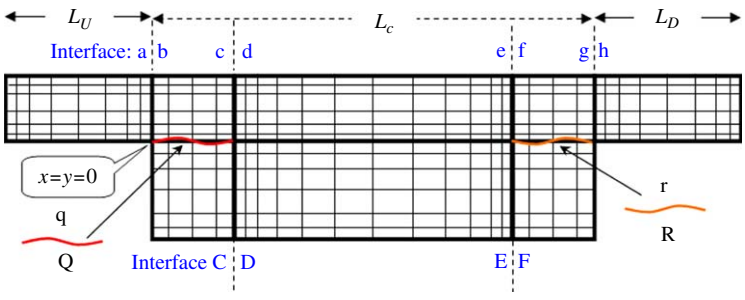

Fig. 5. Computational domain decomposition scheme with all interfaces identified.

solving a large set of equations is eased by domain decomposition with suitable interface matching conditions. For the linear equation with constant coefficients, such as the one being tackled here,

$$\left(\frac{\partial^2}{\partial x^2}+\frac{\partial^2}{\partial y^2}\right)p+k^2p=0, \tag{18}$$

the procedure of Bartels and Stewart [19] is used to reduce the 2D problem into a two-step, 1D problem without iterations required in methods like the ADI scheme.

For each sub-domain with one or more interfaces where values of dependent variables are unknown, the matrix of influence is obtained in a procedure described below using the upstream domain from $x=-L_U$ to 0 as an example. In this domain, the right-hand side interface a–b has unknown pressure values while the inlet boundary condition is known but inhomogeneous. The upper and lower boundaries are solid walls with $\partial p/\partial y=0$. The problem is divided into two parts. In the first, the interface is assigned the homogeneous boundary condition of $p=0$ along the whole interface 'ab'. The left-hand side boundary condition is the plane out-going wave for the reflected part of the sound pressure,

$$p_{\mathrm{ref}}=p-p_{\mathrm{in}}=-\rho_0c_0(u-u_{\mathrm{in}}),$$

where subscript 'in' denotes the incident wave with a prescribed pressure,

$$p_{\mathrm{in}}=1\times\exp(\mathrm{i}\omega t-\mathrm{i}k_0x)=\rho_0c_0u_{\mathrm{in}}.$$

Hence

$$[\mathrm{i}kp-\partial p/\partial x]_{x=-L_U}=-2\ \exp(+\mathrm{i}k_0L_U). \tag{19}$$

The result of this solution in this domain is denoted by a superscript 'in'. The particle velocity derived from pressure gradient, evaluated at the 'a'-side of the interface 'ab' is denoted by $u_a^{\mathrm{in}}=[-(\rho_0\mathrm{i}\omega)^{-1}\partial p/\partial x]_{x=0-}$ with incident wave condition given in Eq. (19) and $p=0$ at the interface $x=0-$. The second part of the upstream domain problem is one in which the upstream boundary condition takes the homogeneous part of Eq. (19), namely $[\mathrm{i}kp-\partial p/\partial x]_{x=-L_U}=0$, while the downstream interface condition is specified by the perturbation of $p_j=1$ for the grid point of index $j=j_p$ and 0 otherwise, where $j_p=1,2,\ldots,M-1$ is the index of the perturbation point excluding the two end points (domain corners). The Helmholtz equation is solved with the above boundary conditions and the value of $\partial p/\partial x$ at the interface 'a' is collected as the j_pth column of the so-called influence matrix u_a^a of size $M-1\times M-1$, where M is the number of Gauss–Lobatto grid segments for the vertical interface 'ab', the subscript 'a' denotes the location of evaluation, while the superscript 'a' denotes the source of influence. Finally, the actual particle velocity at interface 'a' is assembled as follows:

$$u_a\equiv\frac{-1}{\rho_0\mathrm{i}\omega}\times\left.\frac{\partial p}{\partial x}\right|_{x=0-}=u_a^{\mathrm{in}}+u_a^ap_{ab}, \tag{20a}$$

where $p_{ab}=p|_{x=0-}$ is the unknown, common pressure along interface 'ab' to be determined by a matching condition described below. The above combination of two solutions satisfies the full incident wave condition, Eq. (19). The right-hand side of the interface, 'b', receives the influence of perturbation along 'b' itself, along 'c' and from the upper side of the aperture surface 'q'. Using the same notation system,

$$u_b=u_b^bp_{ab}+u_b^cp_{cd}+u_b^qv_{qQ}, \tag{20b}$$

where $v_{qQ}\equiv\partial\eta/\partial t=\mathrm{i}\omega\eta$ is the vertical vibration velocity of the membrane. The continuity of pressure gradient, or velocity, at 'ab' requires $u_a=u_b$, hence the full matching condition for interface 'ab' becomes

$$(u_b^b-u_a^a)p_{ab}+u_b^cp_{cd}+u_b^qv_{qQ}=u_a^{\mathrm{in}}. \tag{20c}$$

The membrane velocity v_{qQ} is related to the acoustic pressure on the membrane by the vertical momentum equation, $\partial p/\partial y+\rho_0\partial v/\partial t=0$, hence

$$\mathrm{d}^{(y)}p_q+\rho_0\mathrm{i}\omega v_{qQ}=0 \tag{21}$$

on boundary 'q', where $\mathrm{d}^{(y)}$ is the first order, Chebyshev derivative matrix in the y direction. The matching condition for q–Q is different. Here, the aperture dynamics equation can be written as

$$m_0\frac{\partial^2\eta}{\partial t^2}-T_0\frac{\partial^2\eta}{\partial x^2}+B_0\frac{\partial^4\eta}{\partial x^4}+p_q-p_Q=0 \tag{22}$$

which can be used for membrane by setting $B_0=0$ and for plate by setting $T_0=0$. Eq. (22) is discretized as follows:

$$mi\omega v_{qQ}-T_0/(\mathrm{i}\omega)\mathrm{d}^{(xx)}v_{qQ}+B_0/(\mathrm{i}\omega)\mathrm{d}^{(xxxx)}v_{qQ}+(p_q^qv_{qQ}+p_q^bp_{ab}+p_q^cp_{cd})-(p_Q^Qv_{qQ}+p_Q^Cp_{CD})=0,$$

where $\mathrm{d}^{(xx)}$, $\mathrm{d}^{(xxxx)}$ are the second and fourth-order derivative matrices, respectively, and p_q^q is the influence matrix (pressure) calculated on 'q' by the boundary condition of Eq. (21) with perturbations of the vertical velocity v_{qQ}.

The coefficients for v_{qQ} in the above equation may be collected together as one matrix for later convenience,

$$\mathscr{M}_{qQ} = m_0 \mathrm{i}\omega - T_0/(\mathrm{i}\omega)\mathrm{d}^{(xx)} + B_0/(\mathrm{i}\omega)\mathrm{d}^{(xxxx)} + p_q^q - p_Q^Q. \tag{23a}$$

Similar matrix can be defined for the downstream aperture,

$$\mathscr{M}_{rR} = m_0' \mathrm{i}\omega - T_0'/(\mathrm{i}\omega)\mathrm{d}^{(xx)} + B_0'/(\mathrm{i}\omega)\mathrm{d}^{(xxxx)} + p_r^r - p_R^R, \tag{23b}$$

where primes denote the structural properties in the downstream aperture, and they vanish when an open aperture is assumed.

Thus defined, all the matching conditions are collected in a grand matrix form,

$$\begin{bmatrix} u_b^b - u_a^a & u_b^c & \{0\} & \{0\} & \{0\} & \{0\} & u_b^q & \{0\} \\ u_c^b & u_c^c - u_d^d & \{0\} & -u_d^e & \{0\} & \{0\} & u_c^q & \{0\} \\ \{0\} & \{0\} & u_C^C - u_D^D & \{0\} & -u_D^E & \{0\} & u_C^Q & \{0\} \\ \{0\} & u_e^d & \{0\} & u_e^e - u_f^f & \{0\} & -u_f^g & \{0\} & -u_f^r \\ \{0\} & \{0\} & u_E^D & \{0\} & u_E^E - u_F^F & \{0\} & \{0\} & -u_F^R \\ \{0\} & \{0\} & \{0\} & u_g^f & \{0\} & u_g^g - u_h^h & \{0\} & u_g^r \\ p_q^b & p_q^c & -p_Q^C & \{0\} & \{0\} & \{0\} & \mathscr{M}_{qQ} & \{0\} \\ \{0\} & \{0\} & \{0\} & p_r^f & -p_R^F & p_r^g & \{0\} & \mathscr{M}_{rR} \end{bmatrix} \begin{bmatrix} p_{ab} \\ p_{cd} \\ p_{CD} \\ p_{ef} \\ p_{EF} \\ p_{gh} \\ v_{qQ} \\ v_{rR} \end{bmatrix} = \begin{bmatrix} u_a^{in} \\ \{0\} \\ \{0\} \\ \{0\} \\ \{0\} \\ \{0\} \\ \{0\} \\ \{0\} \end{bmatrix}, \tag{24}$$

where {0} denotes a null matrix of suitable size. The total number of degree of freedom is the sum of all interface nodes. Numerical tests show that, typically, 8 Gauss–Lobatto segments is quite sufficient for one wavelength. The size of the matrix in Eq. (24) is then very moderate, and no iteration method is required for its solution. Details of the mesh convergence test are described after one numerical example is presented below to allow a better appreciation of the choice of parameters for the test. The above method of Chebyshev Collocation with domain decomposition is abbreviated as the 'ChC' method, or '2D', in the following discussions.

Fig. 6(a) compares the results of the ChC method with the 1D, plane-wave approximation described in Section 2, denoted by '1D' in the legend (dashed line). For the 1D prediction, the parameters are based on Eq. (17) but with membrane tension T set at 0.017 for a twin-aperture design, each with a mass of $m = 0.25$. This level of tension is chosen such that the TL trough is lifted above 10 dB. For the ChC method, a cavity length of $L_c = L_d + L_m = 5h$ is considered to be roughly equivalent to the passage length of $L_d = 4h$ used in the 1D approximation. All other parameters are the same as Eq. (17). For the same tension of $T = 0.017$, the ChC prediction (thick solid line) gives a trough significantly higher than 10 dB. So, a lower level of $T = 0.013$ (thin solid line) is chosen to achieve the same level of trough. The overall TL pattern is similar in the low frequency region despite the obvious frequency shift of the first resonance peak, which may be partly attributed to by the

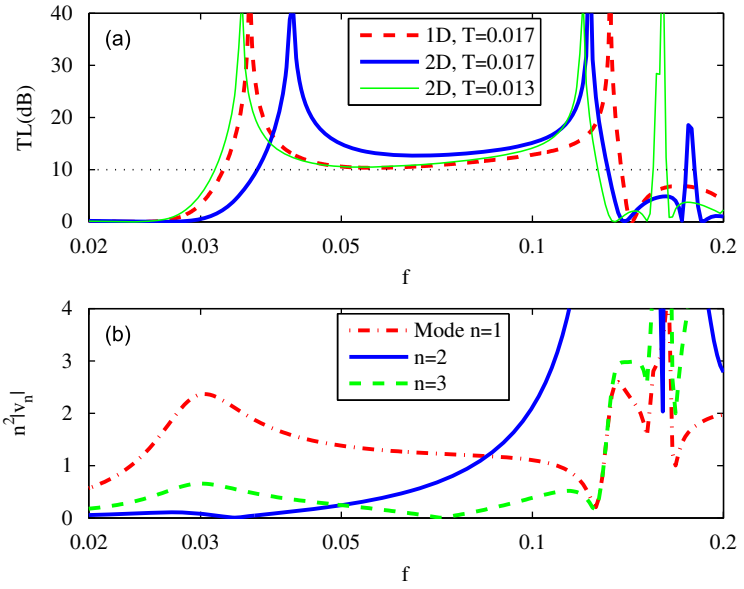

Fig. 6. Comparison between 2D and 1D predictions with parameter setting of (14): (a) transmission loss and (b) analysis of the higher order plate vibration by the 2D prediction.

geometric mismatch between $L_d = 4h$ for the 1D method and $L_c = 5h$ for the 2D method. In the region around and beyond the second peak, however, the difference in the TL pattern and the frequency shift are more pronounced. Note that the 1D theory is not expected to work well in regions with relatively high frequencies.

The membrane vibration mode is studied in Fig. 6(b) for the case of $T = 0.013$ only. Here, the vibration velocity $\partial\eta/\partial t$ is expanded into *in vacuo* modes with amplitude v_n,

$$v_n = \frac{2}{L_m}\int_0^{L_m} \frac{\partial \eta}{\partial t}\sin(n\pi x/L_m)\,\mathrm{d}x.$$

The contribution of each mode towards resisting membrane deformation may be analysed in terms of $n^2|v_n|$ since the tensile restoring force, $T\partial^2\eta/\partial x^2$, is proportional to n^2 for each mode. It is found that the contribution of the third mode (dashed line) is significant in the very low frequency region, while the second mode (solid line) is more important for $f > 0.05$. The contribution of the higher order modes means that the membrane is actually stronger than what the single-mode approximation implies in Section 2, and that essentially explains the frequency shift in Fig. 6(a). Having said this, the single-mode approximation still serves the useful purpose of bringing out the important physics shown by Eqs. (13) and (15).

With the perspective of typical results in Fig. 6(a), the mesh test is now described. The computation domains for Fig. 6(a) have an upstream and downstream domain length of $L_U = L_D = 2.5h$. The number of Gauss–Lobatto grid is $M = 8$ segments across the cavity depth and 4 for half of the duct height. The mesh density is set to be almost the same in the horizontal direction in regions with solid walls but higher density is prescribed for the apertures. A total of 100 segments are used for the whole length of the duct passage. The size of the matrix in Eq. (24) is 56. Mesh convergence test is conducted by varying M while the relative mesh density in various domains is kept unchanged. For the twin-aperture design to be discussed below with $m = 0.25$ and $T = 0.013$ for each membrane, the TL for two typical frequencies of $f = 0.1$ and 0.2 are calculated for $M = 4$, 6, 8, 10, 12 and 16, respectively. Using the results with $M = 16$ as the accurate solution, which are TL = 14.7571, 0.9077 dB for the two frequencies, the deviation of the results from the coarser meshes from these values are given below in the following order $M = 4$, 6, 8, 10 and 12,

$$f = 0.1: \quad \Delta\mathrm{TL} = -1.6\times10^{-2}, 3.2\times10^{-4}, 8.1\times10^{-5}, 1.3\times10^{-5}, 2.7\times10^{-6};$$
$$f = 0.2: \quad \Delta\mathrm{TL} = -4.3\times10^{-2}, -1.8\times10^{-3}, -9.7\times10^{-5}, -7.7\times10^{-6}.$$

The rapid convergence is clearly shown. The mesh density of $M = 8$ is considered to be sufficient and is used in all subsequent examples.

In the 1D approximation, Eqs. (2a) and (3), the denominator $im_0(\omega - \omega_1^2/\omega)$ can be seen as a lumped acoustic impedance for the aperture. For the same mass ratio m_0 and first-mode frequency ω_1, a plate is expected to have the same performance as a membrane according to the 1D approximation. This equivalence is now examined by the full numerical

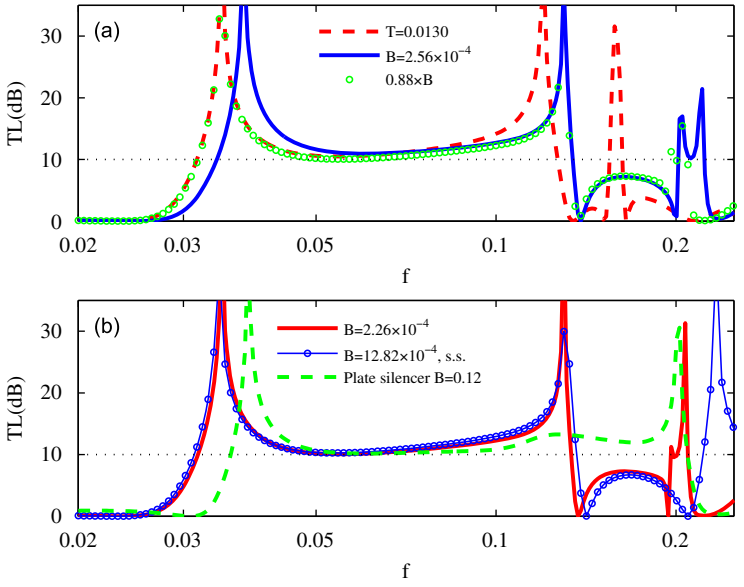

Fig. 7. Comparison between membrane and plate designs: (a) two-aperture design using membrane with $T = 0.013$ and plates with equivalent level of $B = 2.56\times10^{-4}$ and $0.88B = 2.26\times10^{-4}$, all with mass $m = 0.25$ and (b) twin-plate design with $B = 2.26\times10^{-4}$ as used in (a), simply supported plates with $B = 12.82\times10^{-4}$, and plate silencer with $B = 0.12$ [13], also with $m = 0.25$.

prediction, and the results are shown in Fig. 7. To achieve the same ω_1 given by Eqs. (2b) and (3), the plate stiffness B and membrane tension T should be related by the following expressions:

$$\omega_1 = \frac{(1.5056\pi)^2}{L_m^2}\sqrt{\frac{B_0}{m_0}} = \frac{\pi}{L_m}\sqrt{\frac{T_0}{m_0}}, \quad T_0 = B_0\frac{1.5056^4\pi^2}{L_m^2}.$$

In terms of the dimensionless parameters defined in Eq. (16),

$$\frac{T}{B} = \frac{T_0h^2}{B_0} = \frac{1.5056^4\pi^2}{(L_m/h)^2}. \tag{25}$$

For the two-membrane design with $T = 0.013$, and $L_m = h$ used in Fig. 6, the equivalent dimensionless stiffness is $B = 2.56 \times 10^{-4}$. Fig. 7(a) shows that the result for such a two-plate design (solid line) is very similar to that of the two-membrane design (dashed line) with a right-shift of frequencies. The shift indicates the difference in which the higher order modes of the aperture dynamics influence the outcome for the membranes and the plates. This shift in the low frequency region is eliminated when B is reduced to 88 percent of the equivalent B predicted by Eq. (25). The result is shown in open circles. It is interesting to note that the TL for the reduced B also coincides with the plate aperture (solid line) in the high frequency region instead of conforming to the membrane aperture entirely. In other words, the performance of the reduced B takes the best of the two other designs and gives the widest stop-band.

Fig. 7(b) compares three types of plate designs. The thick solid line is for the plate aperture with the reduced B shown in Fig. 7(a), which has the best performance in that group. The line with open circles is also for the twin-plate design but with simply supported boundary conditions at both ends, which requires a higher value of $B = 12.82 \times 10^{-4}$ to clear the 10 dB threshold. The TL curve is almost the same as the clamped plate aperture. The mass ratios for both designs are 0.25. Finally, the performance of the optimal plate silencer [13], namely a single plate covering the whole cavity length of $L_c = 5h$ with air in the cavity, is included as the dashed line for comparison. The mass ratio used for this plate silencer is also $m = 0.25$, its boundary condition is also simply supported, and the optimal bending stiffness to achieve a broad stop-band is $B = 0.12$. This optimal bending stiffness can be reduced when a clamped, non-uniform plate is used [14], but it is structurally much more complicated. The bending stiffness for the plate silencer is about $0.12/0.001282 = 94$ times higher than that for the twin-plate, flute-like silencer of the same geometry. However, when the mass ratio is increased, say to 1.0, the flute-like silencer would suffer performance reductions while the performance of the plate silencer is less sensitive to changes in m provided that m is not too high. More detailed discussion on the material property is given below.

The reason why the cavity is filled with a light gas like helium is two-fold. First, its fast speed of sound than air creates the type-1 HQ resonance. Obviously, a gas with a speed of sound lower than that in air, or a long bypass filled with air, can do the same job. The second function of the light gas is its low inertia. This can be seen in Eqs. (13b) and (15) where the cavity inertia term is lumped together with other system inertia terms in the denominator for the first resonance frequency approximation. Judging from this expression, an increased gas density may be compensated by a smaller aperture mass. This proposition is tested and the results are shown in Fig. 8 where the TL spectra of various membrane masses are compared. The baseline case of helium cavity with twin-membrane design of $m = 0.25$, $T = 0.013$ is shown in a thin solid line. When the cavity gas is replaced by a gas of density $\rho_c/\rho_0 = 0.3$ and its corresponding speed of sound of $c_c/c_0 = 1.543$ with $\gamma = 7/5$, such that the same static pressure $P = \gamma\rho_c c_c^2$ is maintained, the trough of the TL curve (thick solid line) is

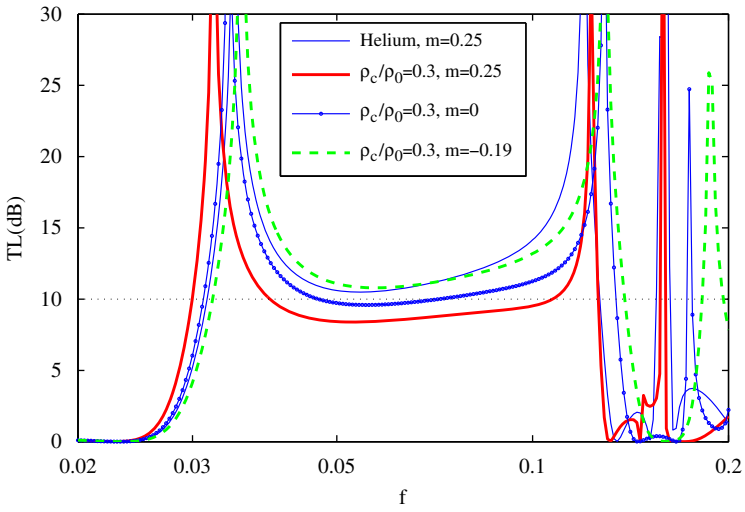

Fig. 8. Effect of cavity gas density on the TL trough level. The flute-like silencer is of the twin-membrane design with tensile stress of $T = 0.013$ is used for all cases.

pulled down below 10 dB. When the membrane mass is reduced to 0 (the line with open circles), the trough is raised but is still below 10 dB. When m is further reduced to -0.19 (dashed line), a level that would make the denominator of Eq. (15) the same as that of the helium cavity, the trough is raised further up and the whole TL pattern is very similar to that of the helium cavity. Note that the change of speed of sound in the cavity causes the resonance frequencies to shift. In fact, the system performance at frequencies just above the first resonance peak is dominated by the system mass, and a reduced system mass can enhance the wave reflection performance.

Before concluding this section, it is useful to discuss the dimensional material properties implied by the predicted dimensionless parameters. Based on the dimensionless mass, tension and stiffness defined in Eq. (16), the dimensional tensile stress σ and Young's modulus E are derived below using the membrane or plate thickness $s = m\rho_0 h/\rho_m$ and a unit width (in the direction perpendicular to the 2D plane) for the membrane or plate,

$$T_0 = T\rho_0 c_0^2 h, \quad \sigma = \frac{T_0}{s} = \frac{T\rho_0 c_0^2 h\rho_m}{m\rho_0 h} = \frac{T}{m}\rho_m c_0^2,$$

$$B_0 = B\rho_0 c_0^2 h^3 = \frac{1}{12}Es^3, \quad E = \frac{12B}{m} \times \frac{\rho_m^3}{\rho_0^3}\rho_0 c_0^2.$$

Since the required dimensionless values for T/m and B/m are high, the crucial parameter for a membrane material is its tensile strength over density, $\sigma_{\max}/\rho_m$, and that for a plate is E/ρ_m^3. Exotic materials such as PVC foams exist but it is more convenient to use usual metal alloys as their properties are more easily quantified and the material more readily available. Aluminum alloy is used here for its reasonable tensile strength (max$\sim$500 MPa) and Young's modulus ($\sim$70 GPa) considering its light weight. For the earlier study of drum-like silencer with the same cavity geometry as used here, the dimensionless tensile stress required for $m = 1$ is $T = 0.475$. This gives a stress level of $\sigma = (T/m)\rho_m c_0^2 = (0.475/1) \times 2700 \times 340^2$ Pa, or 148 MPa, which is within the ideal tensile strength of the best alloy in the aluminum group, but it may exceed the practical limit of some of them due to impurity etc. For plate silencer, earlier study [13] requires $B = 0.1291$ for $m = 1$, and this is translated into $E = 2.35 \times 10^{15}$ Pa, which is 33 557 times the available Young's modulus of aluminum.

In the current study, the membrane tension is much reduced, take $m = 0.25, T = 0.013$ for example, the required dimensional stress is 16.23 MPa, less than 10 percent of the level required in the drum-like silencer. For the two-plate aperture design, the requirement of $m = 0.25, B = 2.26 \times 10^{-4}$ means a Young's modulus of 16 450 GPa, which is 235 times the current material limit. In summary, the twin-membrane design has reduced the requirement on the tensile strength as well as the actual tensile force required, while the plate design is still beyond the reach of common bulk materials.

4. Conclusions

1. When a light gas fills a bypass cavity, its faster speed of sound creates a traditional Herschel–Quincke resonance in which the temporal path difference between the main duct segment and the bypass is equal to half of an oscillation period. The nature of the HQ resonance means that it is not suitable for the abatement of very low frequencies due to its long wavelength.
2. When the bypass is covered by two impervious membrane apertures, so that the light gas may not leak out, the system exhibits another resonance which can be located at very low frequencies. The frequency is determined by the tensile stress applied on the membrane and the system mass which includes three contributions: the air in the main duct, the gas in the cavity and the membrane mass. The resonance is similar to the second type of HQ resonance in which the combined acoustic path in the duct and bypass forms full periods (when they have the same cross section). The mechanism differs from the earlier use of helium in a drum-like silencer [11].
3. The transmission loss performance depends crucially on the trough between the two resonance peaks. Since resonance peaks are frequencies where the system mass balances system stiffness, which can be written symbolically as $mi\omega + K/i\omega = 0$, the system performance between two neighbouring peaks depends on the imbalance of the two effects when frequency deviates from the resonance frequency. When both mass and stiffness are low, the imbalance would be maintained at a low level and system performance would be high. When the cavity is filled with a light gas, the required tension is very low for a given system mass. The low tension helps the low frequency performance. The low gas density helps the system performance from medium to high frequencies. Together, the system impedance seen by the incident wave is maintained at a low level, and the trough between the two resonance peaks can be elevated to a certain high level.
4. The device, which is called a flute-like silencer featuring two identical membrane or plate apertures, is found to perform well in the low frequency region when compared with the drum-like silencer [12] and plate silencer [13] developed earlier. The transmission loss spectrum features two peaks, contrasting with the three-peak spectrum seen in the drum-like or plate silencers. The very short aperture length means that the required membrane tension, or plate stiffness, is much lower than those required in the drum-like or plate silencer. For the membrane design, the parametric study shows that it is well within the material limits while the plate aperture is still beyond the limits of existing bulk materials.

Acknowledgement

The author would like to acknowledge the support from the seed fund for applied research from the University of Hong Kong.

References

[1] L.L. Beranek, Criteria for noise in buildings and communities, in: I.L. Ver, L.L. Beranek (Eds.), *Noise and Vibration Control Engineering: Principles and Applications*, second ed., Wiley, New York, 2006 (Chapter 20).
[2] M.L. Munjal, A.G. Galaitsis, L.L. Ver, Passive silencers, in: I.L. Ver, L.L. Beranek (Eds.), *Noise and Vibration Control Engineering: Principles and Applications*, second ed., Wiley, New York, 2006 (Chapter 9).
[3] W.E. Blazier, RC mark II: a refined procedure for rating the noise of heating, ventilating, and air-conditioning (HVAC) systems in buildings, *Noise Control Engineering Journal* 45 (1997) 243–250.
[4] H.V. Fuchs, X. Zha, H. Drotleff, Relevance and treatment of the low frequency domain for noise control and acoustic comfort in rooms, *Acta Acustica United with Acustica* 91 (2005) 920–928.
[5] S. Brown, Acoustic design of broadcasting studios, *Journal of Sound and Vibration* 1 (1964) 239–257.
[6] R.D. Ford, M.A. McCormick, Panel sound absorbers, *Journal of Sound and Vibration* 10 (1969) 411–423.
[7] U. Ackermann, H.V. Fuchs, N. Rambausek, Sound absorbers of a novel membrane construction, *Applied Acoustics* 25 (1988) 197–215.
[8] L. Huang, A theory of passive duct noise control by flexible panels, *Journal of the Acoustical Society of America* 106 (1999) 1801–1809.
[9] L. Huang, Modal analysis of a drum-like silencer, *Journal of the Acoustical Society of America* 112 (2002) 2014–2025.
[10] Y.S. Choy, L. Huang, Experimental studies of a drum-like silencer, *Journal of the Acoustical Society of America* 112 (2002) 2026–2035.
[11] Y.S. Choy, L. Huang, Drum silencer with shallow cavity filled with helium, *Journal of the Acoustical Society of America* 114 (2003) 1477–1486.
[12] L. Huang, Parametric study of a drum-like silencer, *Journal of Sound and Vibration* 269 (2004) 467–488.
[13] L. Huang, Broadband sound reflection by plates covering side-branch cavities in a duct, *Journal of the Acoustical Society of America* 119 (2006) 2628–2638.
[14] C. Wang, J. Han, L. Huang, Optimization of a clamped plate silencer, *Journal of the Acoustical Society of America* 121 (2007) 949–960.
[15] G.W. Stewart, The theory of the Herschel–Quincke tube, *Physical Review* 31 (1928) 696–698.
[16] A. Selamet, N.S. Dickey, The Herschel–Quincke tube: a theoretical computational and experimental investigation, *Journal of the Acoustical Society of America* 96 (1994) 3177–3185.
[17] J.P. Boyd, *Chebyshev and Fourier Spectral Methods*, second ed., Dover, New York, 2001.
[18] L. Huang, Membrane covered duct lining for high-frequency noise attenuation: prediction using a Chebyshev collocation method, *Journal of the Acoustical Society of America* 124 (2008) 2918–2929.
[19] R.H. Bartels, G.W. Stewart, Algorithm 432: solution of the matrix equation $AX+XB=C$, *Communications of the ACM* 15 (1972) 820–826.